

DTT device: Conceptual design of the superconducting magnet system

Original

DTT device: Conceptual design of the superconducting magnet system / Di Zenobio, A.; Albanese, R.; Anemona, A.; Biancolini, M. E.; Bonifetto, Roberto; Brutti, C.; Corato, V.; Crisanti, F.; della Corte, A.; De Marzi, G.; Fiamozzi Zignani, C.; Giorgetti, F.; Messina, G.; Muzzi, L.; Savoldi, Laura; Tomassetti, G.; Turtù, S.; Villone, F.; Zappatore, Andrea. - In: FUSION ENGINEERING AND DESIGN. - ISSN 0920-3796. - STAMPA. - 122:(2017), pp. 299-312.
[10.1016/j.fusengdes.2017.03.102]

Availability:

This version is available at: 11583/2667423 since: 2018-01-31T00:04:08Z

Publisher:

Elsevier

Published

DOI:10.1016/j.fusengdes.2017.03.102

Terms of use:

This article is made available under terms and conditions as specified in the corresponding bibliographic description in the repository

Publisher copyright

Elsevier postprint/Author's Accepted Manuscript

© 2017. This manuscript version is made available under the CC-BY-NC-ND 4.0 license
<http://creativecommons.org/licenses/by-nc-nd/4.0/>. The final authenticated version is available online at:
<http://dx.doi.org/10.1016/j.fusengdes.2017.03.102>

(Article begins on next page)

DTT Device: conceptual design of the superconducting magnet system

A. Di Zenobio^(a), R. Albanese^(c), A. Anemona^(a), M. E. Biancolini^(b), R. Bonifetto^(e), C. Brutti^(b), V. Corato^(a), F. Crisanti^(a), A. della Corte^(a), G. De Marzi^(a), C. Fiamozzi Zignani^(a), F. Giorgetti^(b), G. Messina^(a), L. Muzzi^(a), L. Savoldi Richard^(e), G. Tomassetti^(a), S. Turtù^(a), F. Villone^(d), A. Zappatore^(e)

^(a) = ENEA, Via E. Fermi 45, 00044 Frascati (RM) – ITALY

^(b) = Università di Roma Tor Vergata, Via del Politecnico 1, 00133 Roma (RM), ITALY

^(c) = Consorzio CREATE, DIETI – Università di Napoli Federico II, Via Claudio 21, I-80125 Napoli (NA), ITALY

^(d) = Consorzio CREATE, DIEI, Università degli Studi di Cassino e del Lazio Meridionale, Cassino (FR), ITALY

^(e) = NEMO group, Dipartimento Energia, Politecnico di Torino (TO), ITALY

Corresponding author: Aldo Di Zenobio, ENEA – aldo.dizenobio@enea.it

Abstract

In the European Fusion Roadmap, one of the main challenges to be faced is the risk mitigation related to the impossibility of directly extrapolate to DEMO the divertor solution adopted in ITER, due to the very large loads expected. Thus, a satellite experimental facility oriented toward the exploration of robust divertor solutions for power and particles exhaust and to the study of plasma-material interaction scaled to long pulse operation, is currently being designed. Clearly, design requirements for this experiment are quite challenging, to account for the extreme operation conditions, which shall be as representative as possible of the DEMO ones, but in a much smaller device and at lower costs. A feasibility assessment has been carried out for the fully superconducting magnet system of the compact Divertor Tokamak Test (DTT) facility project. The overall magnet system is based on NbTi and Nb₃Sn Cable-in-Conduit Conductors, and it adopts some of the most recent developments in this field. It consists of 18 Toroidal Field (TF), 6 Poloidal Field (PF) and 6 Central Solenoid (CS) module coils. In order to cope with the machine requirements such as plasma major and minor radii, magnetic field on plasma axis, plasma current, and inductive flux requirement, the Nb₃Sn TF coil is characterized by a peak field of 11.4 T on the conductor, operating at 46.3 kA; the Nb₃Sn CS modules are characterized by a peak field of about 13 T, with a conductor operating current of 23 kA; the PF coils are wound using NbTi conductors operating at a maximum peak field of 4.0 T, with operating currents in the range 21 kA to 25 kA, depending on the PF coil. Profiting of the compact machine size, and thus of relatively short conductor lengths, the TF coil winding pack is conceived as layer wound and made of two distinct sections, a low- and a high-field one, employing different superconductor cross-sections, and electrically connected through an embedded “ENEA-type” joint. The main features of the magnet system are described here; the results of mechanical, electrical and thermo-hydraulic analyses, which are discussed here, indicate that the proposed design fulfills all the required criteria. In addition, a brief description of the In-Vessel coils is given, though they are not superconducting, for the sake of completeness.

Keywords: fusion, tokamak, divertor, superconductivity, magnets

INDEX

Introduction	3
1 DTT Toroidal Field coil system	3
1.1 Toroidal Field Conductor design.....	5
1.2 TF - 1D thermo-hydraulic analysis.....	7
1.2.1 4C model of the DTT TF WP	7
1.2.2 Results	8
1.3 TF - Mechanical loads	9
1.3.1 3D mechanical analysis	9
1.3.2 2D mechanical analysis	10
1.4 TF - Inductance calculation	10
1.5 TF - ripple.....	11
2 DTT Poloidal Field coil system	12
2.1 CS coil description	12
2.2 CS - AC losses.....	14
2.3 CS - mechanical analysis.....	15
2.4 PF - description	16
2.5 CS & PF - magnetic field analysis	16
2.6 In-Vessel copper Coils	17
Conclusions	18
References	19

Introduction

The development of a reliable solution to manage power and particle exhaust in a tokamak reactor is considered one of the major challenges towards the realization of a nuclear fusion power plant [1]. The DTT (Divertor Tokamak Test) facility is being proposed in Europe, with the aim to explore different divertor configurations in ranges as representative as possible of the DEMO ones [1], [2], [3], even if scaled to a much smaller and compact device. Results of such tests should help to cover the gap between the solutions that will be tested in ITER and those to be adopted in DEMO. The DTT tokamak device is characterized by a plasma major radius of 2.15 m, an aspect ratio $R/a = 3.1$ and a relatively high toroidal field on plasma axis: $B_{\text{plasma-axis}} = 6$ T. Plasma scenarios are characterized by a pulse length of 100 s or more, with a plasma current of 6 MA, to be achieved with a Central Solenoid swing of 35 Vs.

Based on these requirements, the DTT magnet system which has been conceived in order to verify the feasibility of this machine, consists of a set of superconducting coils, wound by Cable-In-Conduit Conductors (CICCs), constituted of the low temperature superconducting (SC) materials Nb_3Sn (for the 18 Toroidal Field coils and the 6 Central Solenoid modules) and NbTi (for the 6 Poloidal Field coils). Also, 8 In-Vessel copper coils are foreseen, for plasma radial and vertical stabilization and control, as well as for magnetic control of charged particles impinging on the divertor target plates. The artistic sketch of Figure I reports a sector of the DTT machine, where the shape of the Toroidal Field (TF) coils and their inter-coil structures are shown, together with the 6 Poloidal Field (PF) coils, and the plasma shape. The layout of the ports for the access to the vacuum vessel, and the layout of the gravity supports are also shown, along with a partial view of the 6 Central Solenoid (CS) modules and their support.

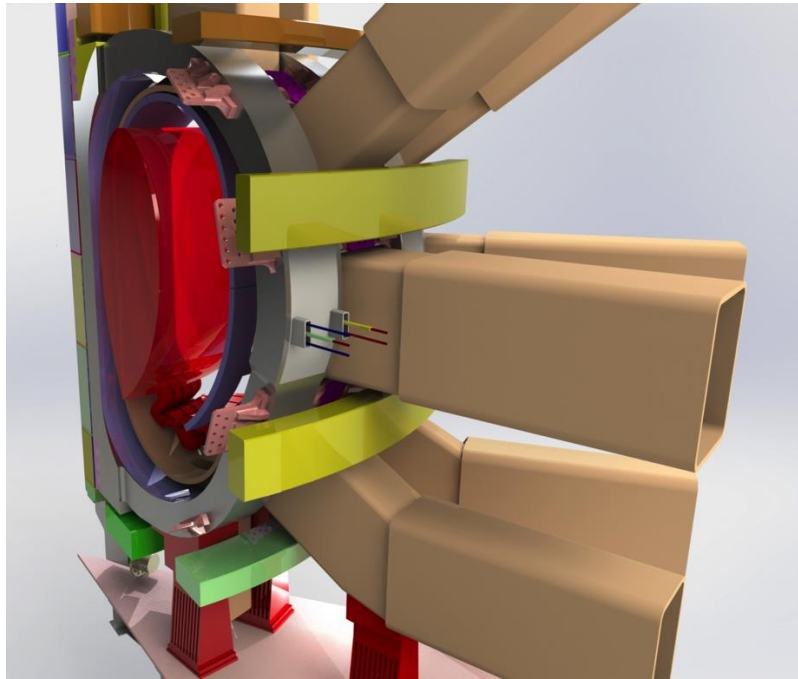


Figure I: sketch of the DTT device, with the magnet system, the plasma shape and the ports.

1 DTT Toroidal Field coil system

The Toroidal Field system consists of 18 coils, and its design is driven by the constraints of the machine dimensions, the TF coil outer dimensions being about 3.5 m x 5.0 m, and of the requested field at the plasma axis, i.e. $B_{\text{plasma-axis}} = 6.0$ T @ $R = 2.15$ m. The total current flowing in the 18 coils system is: 65 MA.

The TF coil winding pack (WP), as shown in Figure II, is made by 78 turns of Nb_3Sn Cable-in-Conduit conductors, each carrying an operative current $I_{\text{op}} = 46.3$ kA and cooled by a forced flow of supercritical Helium, having an inlet temperature $T_{\text{in}} = 4.5$ K. In order to optimize the space allocation for the stainless steel and for the superconducting material, the winding pack is designed in a graded solution, combining two different Nb_3Sn

conductor layouts (see Figure II). As computed by the 3D TOSCA[®] code, the high-field (HF) plasma-facing section is characterized by a peak field $B_{\text{peak-HF}}$: 11.4 T and it is wound by a rectangular conductor with 2.5 mm thick steel jacket; on the other hand, the low-field (LF) outermost section is subject to a maximum field $B_{\text{peak-LF}}$: 7.6 T, and it is therefore characterized by a smaller superconductor cross-section and a thicker steel jacket, of 3.7 mm, which is required to sustain the accumulating load of the TF coil centring force. This solution allows for an optimization of both the superconductor and the steel cross-section in the winding pack, with respect to a solution based on pancake-winding [4], [5], as the one adopted for example in ITER. Being the hydraulic lengths relatively short, the layer-winding solution may be chosen so to reduce the number of internal joints, with respect to the pancake layout.

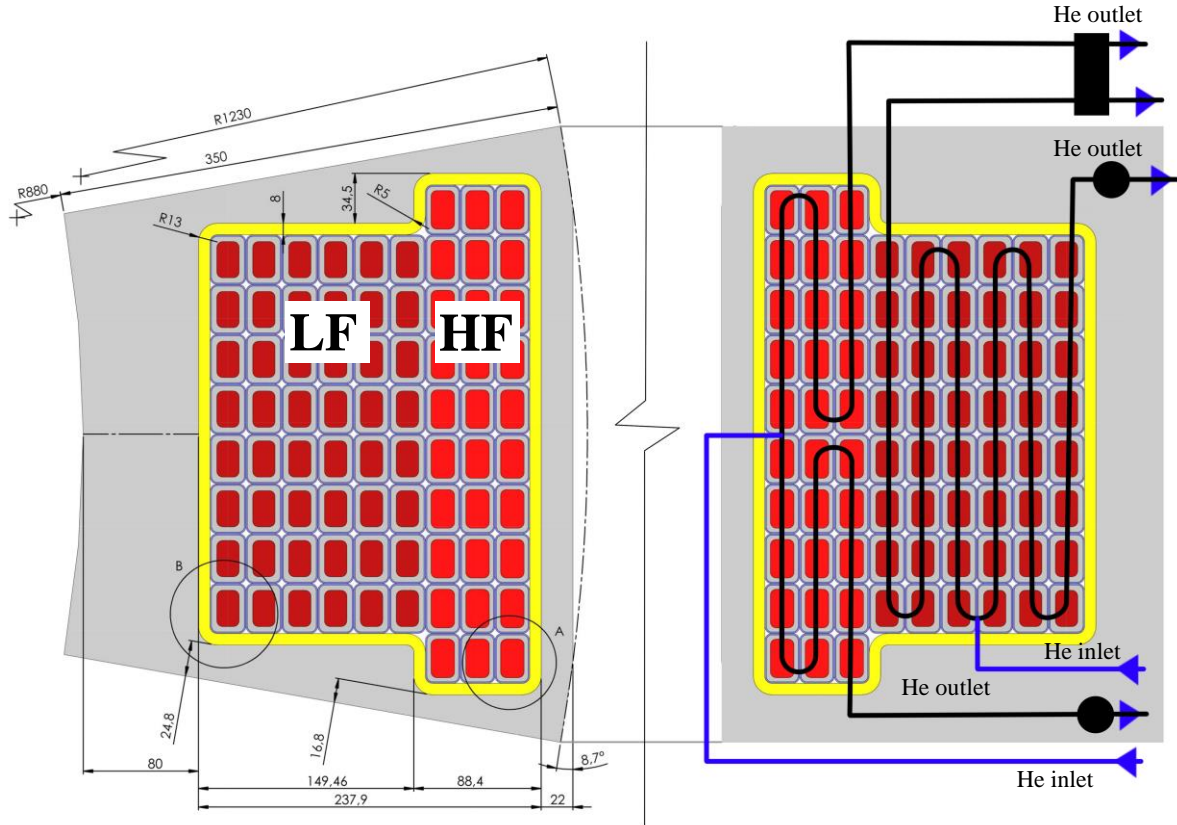


Figure II: the DTT TF Winding Pack and casing cross-section at the inner leg (left) and outer leg (right). The 3 innermost turns are the HF sections, whereas the outermost turns constitute the LF one. The arrows indicate the schematic path of the circulating cooling Helium (2 inlets and 3 outlets); the black circles indicate the 2 electrical terminations; the black box the inner inter-layer embedded joint.

The graded solution can be adopted by winding the TF coil in layers, starting from the innermost module, made of 3 layers x 20 turns, and then continuously winding over it the LF section, made of 6 layers x 8 turns. The proposed winding layout is, to the best knowledge of the authors, quite innovative. It has been studied in details, and did not show any major issue, as far as mechanics, thermo-hydraulics and electrical insulation are concerned, as shown in the analyses and comments reported below. The two modules are connected by an “ENEAT-type” joint [6], manufactured in-line during the winding operation and totally embedded within the winding pack space. This technique was already successfully used for the manufacture of the EDIPO Nb₃Sn coil [7], the NAFASSY Nb₃Sn coil [8] and, with some variations, for the ITER Central Solenoid coils [9]. Both the HF and the LF sections are divided into 2 symmetric hydraulic paths. For the HF section, the He inlet is placed on the innermost plasma-facing layer, at the middle length of the conductor length, whereas for the LF it is placed on the side of the WP between the 3th and 4th layer. The 3 outlets are obviously placed at the joint and the 2 terminations (see Figure II). As can be inferred from Figure I, the hydraulic and electrical connection (coil terminations) lie on the outboard region of the coil, close to the equatorial plane, in the space available between the two larger PF coils.

During winding operation, the conductor is wrapped in-line by a 1 mm thick fiberglass tape. The whole WP will be then additionally wrapped with 3 mm thick fiberglass. The resulting coil is subject to the heat treatment necessary to reach the Nb₃Sn reaction and then to a Vacuum Pressure Impregnation, so to obtain a fiberglass

reinforced epoxy resin. An additional gap of 5 mm is left for casing operations (insertion of the complete and heat-treated WP into the SS case). This gap will be filled again by fiberglass material and then the whole coil will be subject to a second Vacuum Pressure Impregnation process. In this way the TF coil will have a ground insulation thickness of 8 mm and a 2 mm inter-turn insulation. Preliminary calculations showed this thickness to be sufficient to face the maximum foreseen voltage ($< 3\text{kV}$), but further checks are on-going to verify if more or different material may be advised.

The TF coils are designed to work in wedging configuration over their inner straight sections to support the in-plane centring forces. The TF casing will be actively cooled, in order to reduce the heat transfer to the superconductors, especially due to the neutron load over the stainless steel (SS). The design of the layout and positioning of the active cooling channels in the casing has not been finalized yet, and thus they are not shown in Figure II.

The TF coil casing is bolted to a gravity support, which is fixed to the cryostat base. The gravity support of each coil, enveloped in a thermal shield, also sustains the weight of the CS modules and of the 6 PF coils. Finally, the TF casing acts also as a base for the shelves supporting the outer PF coils, foreseen in a suitable way to allow radial movements when energized (Figure I). The detailed design of these shelves has to be performed.

The main characteristics of the TF coils are summarized in Table 1-I.

TABLE 1-I
TF COIL MAIN CHARACTERISTICS

# turns (1 coil)	78
HF section	3 layers x 10 turns
LF section	6 layers x 8 turns
Ground insulation	8 mm
Inductance (1 TF coil)	41 mH
Inductance (18 TF coil system)	1.5 H
HF /LF lengths	330 m / 560 m
Hydraulic lengths	165 m / 280 m
Mass flow rate (18 coils)	200 g/s
Conductor length for 1 WP	890 m
Total TF conductor length	16 km
Total Nb ₃ Sn strand length	6800 km
Total Cu strand length	9900 km
Casing material	AISI 316L
Weight of 1 TF coil	13 tons
Overall TF coil system weight	235 tons

1.1 Toroidal Field Conductor design

The Toroidal Field conductor relies on an ITER-like Nb₃Sn strand, with 0.82 mm diameter, Cu:nonCu = 1, effective filament diameters below 10 μm , with a slightly enhanced critical current performance: $I_c(4.2\text{ K}, 12\text{ T}, \epsilon_{\text{appl}}=0) = 247\text{ A}$. This choice, demonstrated to be already achievable by the main ITER suppliers, as well as the choice of the parameters retained for the description of the strain sensitivity of the superconducting wire, is the same as the one currently adopted within the DEMO magnets development group [3].

The Cable-in-Conduit conductors adopted for the 2 different graded sections of the WP, are characterized by a rectangular shape with aspect ratio of 1.5 and a low Void Fraction (VF), about 26%, with the aim of optimizing the electromagnetic pressure over the Nb₃Sn strands, whose performance is affected by the strain. The cumulative load over the conductor due to the electromagnetic force is about 530 kN/m and 350 kN/m for the HF and LF CICC respectively. In this sense the rectangular geometry, with the main load component directed perpendicularly to the wide conductor side, contributes in reducing the electromagnetic pressure over the strands. A possible AC losses increase correspondent to this layout has not yet been assessed, considered anyhow to be not critical for TF coils. Differently from what done in the case of the Nb₃Sn ITER Central Solenoid CICC [10], [11], where a very short twist pitch cable configuration was chosen to prevent cable movements during load cycles, a so-called “long twist pitch” cable scheme is retained here as more appropriate to obtain a homogeneous

and regular distribution of wires within the cross-section during the compaction to the rectangular geometry [4]. This design rationale is supported by many studies and tests performed in the past [12], [13], [14], [15] and [16], and taking into account also the large experience gained in relevant projects, like the EDIPO [7], the HFML 45T hybrid magnet project [14], and the DEMO project, where a rectangular, very large-size CICC has been designed and successfully tested at the SPC laboratories in Switzerland [5].

The main characteristics of the HF and LF rectangular conductors are reported in Table 1-II. The two conductors are very similar in size but, as already discussed, are characterized by a different Cu/superconductor fraction, and by a different jacket thickness. Some parameters reported in this table are discussed in the following paragraphs.

TABLE 1-II
TF CONDUCTOR MAIN CHARACTERISTICS

	HF	LF
Outer Dimensions (before insulation)	22.1 x 32.5 mm	22.9 x 32.5 mm
Jacket material	AISI 316LN	
Jacket thickness	2.5 mm	3.7 mm
Inter-turn electrical insulation	2.0 mm (1.0 mm wrap around each conductor)	
# Nb ₃ Sn strands	351	150
# Cu segregated strands	257	354
Cu and Nb ₃ Sn Strand diameter	0.82 mm	
Strand Cu:nonCu ratio	1	
Steel cable wrapping thickness	0.1 mm	
Void Fraction	25.9%	25.3%
Operative Current	46.3 kA	
Non-Cu current density	500 A/mm ²	1170 A/mm ²
He Inlet Temperature	4.5 K	
ΔT_{margin} (after Neutron Load)	0.8 K	1.0 K
T_{hotspot} (Cu and SC only)	245 K	268 K
T_{hotspot} (all materials)	104 K	81 K
Pressure Drop	3.1 bar	
Mass flow rate	3.5 g/s	2 g/s

In order to verify the required copper amount for protection in case of quench, a first estimation of the Hotspot temperature with a simplified adiabatic 0D model [17] has been performed for both conductor grades, with different discharge time constant ($\tau_{\text{discharge}}$) values (ranging between 5 s to 8 s) and with a delay time constant, $\tau_{\text{delay}} = 1$ s. Materials properties have been taken from [18]. As results, the ITER criteria of having a $T_{\text{hotspot}} < 150$ K with all the materials, can be very comfortably satisfied. For the more conservative criteria, i.e. maintaining the $T_{\text{hotspot}} < 250$ K considering only copper and superconducting materials within the cables, the results show that $\tau_{\text{discharge}}$ must be kept at 5 s (Figure III).

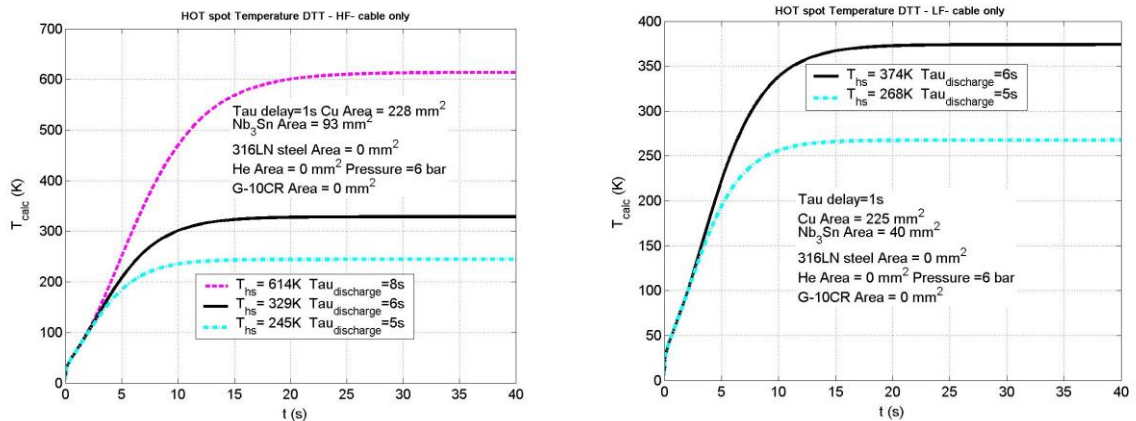


Figure III: Hotspot calculation for DTT TF conductors during a quench, when only Cu and SC cable contents are considered; results for the HF and for the LF CICC are shown on the left and on the right, respectively.

Further analyses are foreseen, to assess the final $\tau_{\text{discharge}}$ and τ_{delay} values, considering more detailed aspects linked to quench detection and quench evolution. Anyhow, it has been calculated that even with a $\tau_{\text{discharge}}$ of 5 s, the single coil voltage does not exceed 500 V and that the Vacuum Vessel is capable to withstand a discharge of all the TF coils as fast as 1.5 s, thus leaving a large margin from this point of view (see also [19]).

1.2 TF - 1D thermo-hydraulic analysis

The thermal-hydraulic analysis of the TF winding pack aims at determining the performance of the coil during the expected plasma operation and it has been performed using the 4C code [20], already successfully applied to the performance analysis of several existing [21] and future [22] experiments.

1.2.1 4C model of the DTT TF WP

The 4 parallel hydraulic channels used to cool the 2 sections of the WP have been modelled as 1D He flow coupled with the solids (namely, strands and jacket) [20]. In the present analysis, the WP has been considered adiabatic with respect to the casing, so that the latter has not been modelled. As represented in Figure IV, the SHe inlets are planned to be positioned at the bottom of the outboard leg: cold He will be supplied to the HF conductor (hydraulic channels 3 and 4, respectively) from the plasma side of the coil and to the LF conductor (hydraulic channels 1 and 2, respectively) from the side of the coil.

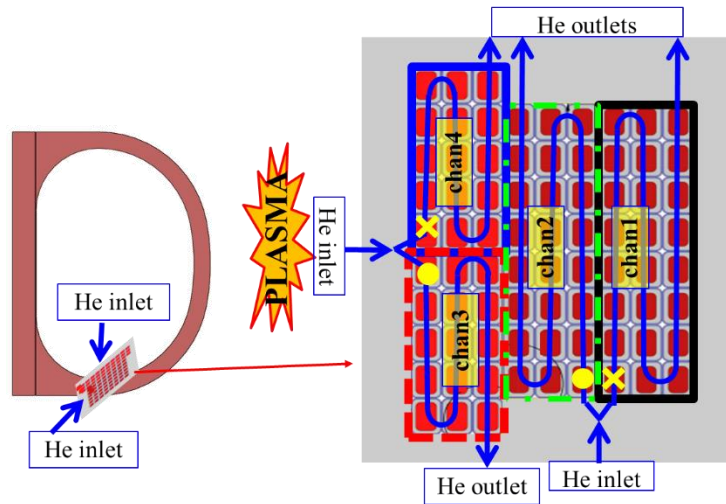


Figure IV: Schematic representation of the positions of the SHe inlets in the D-shaped TF coil (left). Cross section of the TF WP (right) showing the 4 hydraulic channels (black solid, green dash-dotted, red dashed and blue solid boxes) as well as the hydraulic paths (blue solid thin lines) and the detailed view of the SHe inlets/outlets positions in the WP (blue arrows). The yellow crosses and dots represent the direction of the SHe flow.

The inter-turn (IT) and inter-layer (IL) thermal coupling between the hydraulic channels has been taken into account, as well as the co-current / counter-current flow in the different channels.

The boundary conditions adopted for the coolant are: constant inlet temperature (4.5 K), inlet pressure (6 bar) and outlet pressure (2.9 bar). The initial temperature is assumed constant and equal to 4.5 K.

The magnetic field depends on the hydraulic coordinate along each channel [26], with a maximum effective value on the cable axis of ~ 11 T at the first layer inboard equator, and is conservatively kept constant at the end-of-flat-top value during the whole analysis. The nuclear heat (NH) load P [W/m] in each turn has a distribution given by the exponential law $P(x) = 0.8 \times \exp(-5 \times x)$, following the same decay law presented in [27], where x is the radial distance in m from the plasma side of the WP. It is worth noticing here that a conservative approach, i.e. a relatively high value of NH, has been taken into account for the present study, as a detailed analysis of the neutron load has not yet been completed.

The superconductor critical properties are the same as in [25], and the ITER Nb₃Sn scaling [28] is adopted. The modified version of Darcy-Forchheimer friction factor correlation [29] is adopted, as it gave satisfactory agreement with the cold tests results of the JT-60SA TF coils [30], having a conductor geometry similar to the DTT TF coils one.

The input parameters adopted for the analysis are summarized in Table 1-III.

TABLE 1-III
INPUT PARAMETERS FOR THERMO-HYDRAULIC ANALYSIS

# turns	78
# layers	9
HF / LF lengths [m]	330 / 560
HF / LF hydraulic lengths [m]	165 / 280
Mass flow rate in 1 coil (HF / LF) [g/s]	11 (7 / 4)
Current [kA]	46.3
Strand type	ITER-like Nb ₃ Sn ($J_c @ 4.2 \text{ K}; 12 \text{ T}; \epsilon_{\text{applied}}=0$) = 1125 A/mm ²)
Total axial strain [%]	-0.5
RRR (weighted average of SC and Cu strands)	250
Inlet temperature [K]	4.5
Inlet pressure [bar]	6
Outlet pressure [bar]	2.9

1.2.2 Results

The computed results of the temperature margin are presented in Figure V. Both the minimum current sharing temperature and the maximum conductor operating temperature are located in the first layer of the 3rd and 4th channel, see Figure V(a). In particular, the former is due to the magnetic field spatial distribution, and the latter to the radial decay of the NH load, which has its maximum value over the first layer. Precisely, the minimum temperature margin of ~0.8 K, see the inset of Figure V (b), is located at $x = 19.3 \text{ m}$ from the hydraulic inlet of the 3rd channel.

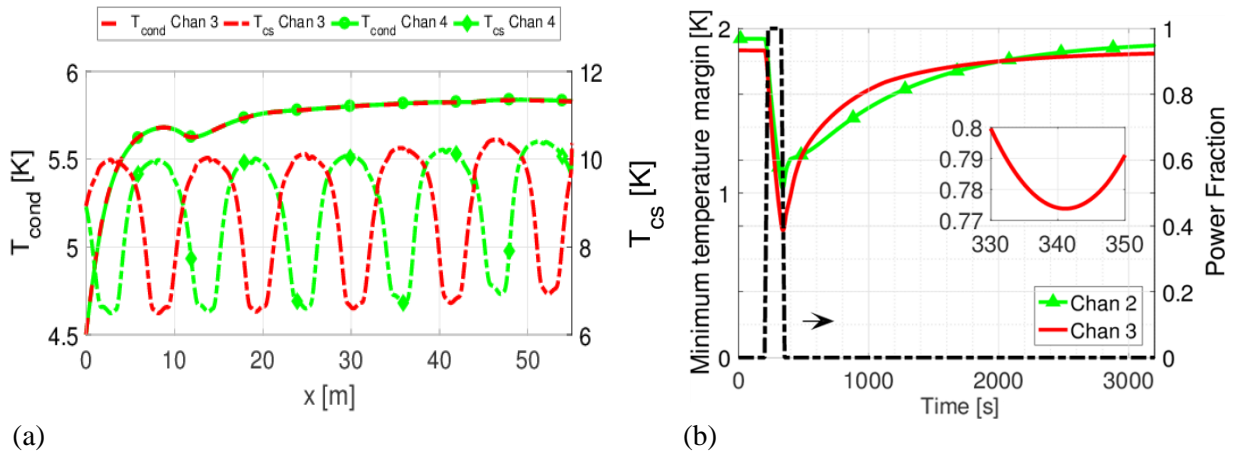


Figure V: Spatial distribution of the conductor and current sharing temperatures in the first layer of the most critical channels 3 and 4 for the nominal case (a). Evolution of the minimum temperature margin in the channels 2 and 3, together with the plasma scenario considered (b).

Figure V(b) shows that minimum temperature margin is reached well after the end of the flat-top, but still slightly before the end of the pulse, meaning that also during the ramp down a considerable amount of power is deposited in the WP. The absolute minimum value is reached in the 3rd hydraulic channel, which anyway behaves very similarly to the 4th. In fact, in both channels the minimum margin is ~0.8 K. The difference between the two is mainly due to the asymmetry of the magnetic field, which implies that the minimum value of the T_{cs} is located closer to the inlet for the 4th channel, see Figure V(a), where the effect of fresh He entering the conductor is present, resulting in a slightly higher minimum temperature margin value.

In order to assess the impact on the computed results of a lower mass flow rate, with respect to the 3.5 g/s obtained in the 3rd and 4th channels, some parametric simulations have been performed (not shown). Even though

the temperature margin is not largely affected by a reduction of the He flow rate, some backflow is likely to occur for a mass flow $< \sim 2$ g/s, which would be a concern during normal operation.

The modelling of the IT/IL thermal coupling is fundamental to properly compute the re-cooling speed of the WP, a favourable condition if repeated pulses with short dwell time are envisaged.

Another relevant effect of the high NH load conservatively adopted for the present study, with respect to e.g. the one on the DEMO TF coils [31], is the computed strong perturbation of the mass flow rate, see Figure VI, which at the inlet (i.e., close to the minimum margin location in the critical channels) can be reduced to below 50% of the nominal value during the plasma burn.

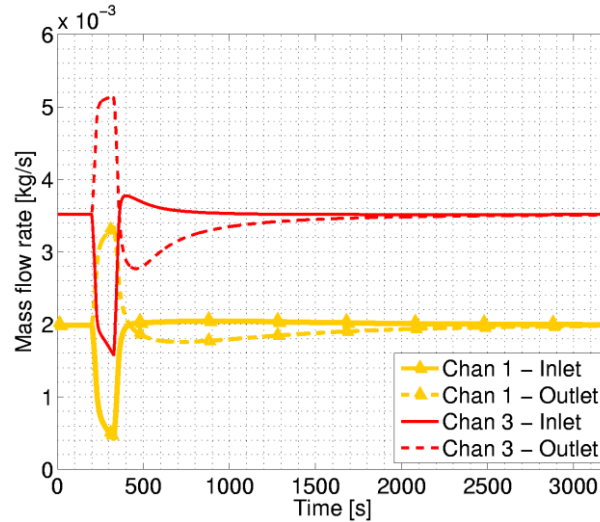


Figure VI: Evolution of the mass flow rate in the channels 1 and 3 for the nominal case.

Further analyses will be performed once a detailed neutron load will be available. Based on what has conservatively been studied so far, it can be stated that the TF conductor has been designed with a sufficient temperature margin.

1.3 TF - Mechanical loads

1.3.1 3D mechanical analysis

Finite element (FE) 3D analysis of the DTT TF coil system has been performed, considering the stresses rising during the energizing of the 18 coils at their operative current. At this stage of the project, no out-of-plane load has been introduced and the effect of cooldown has not been considered, even if material properties have been taken at 4.2 K. The assumed constraint conditions are: frictionless contact at cyclic symmetry surfaces and rigid vertical gravity support to remove lability. Based on such assumptions, an overall 3D Finite Elements model of the coil has been set-up, using a fine mesh with 49161 parabolic tetrahedral elements and 82606 nodes. The software tool used for stress analyses is NX Nastran 8[®], with the pre-post processor FEMAP 10.3[®]. For all material properties, ITER values have been retained [32]. An homogenisation procedure has been applied, to define the smeared material properties of the winding pack. The adopted procedure, based on H. Berger method, allows to retrieve the smeared properties using a representative volume element (RVE). Imposing a deformation to this RVE it is possible to find out the elemental stresses and then the average stress. From the found stress and the imposed strain it is possible to retrieve the equivalent elastic properties of the RVE.

Electromagnetic load has been evaluated by calculating with the TOSCA[®] code the magnetic field components for an optimized data set of more than 3000 points in the TF winding pack; this dataset has been then interpolated using an innovative and fully validated meshless approach, based on Radial Basis Functions (RBF) [33]. This method allows for transforming the scattered data known at source points, as magnetic field and current density, in point functions available everywhere. In this way a Force Density can be defined and used to apply loads on a target distribution (having different size and spacing with respect to the source).

As shown in Figure VII (lower left), the maximum Von Mises stress is located on the steel case structure, in the nose area, where the TF system centring force accumulates. The maximum value is < 650 MPa, and therefore not critical, even if the effect of the out-of-plane loads is still missing within the present analysis, and will be critically evaluated. The maximum radial displacements computed at the equatorial plane within this global model are: -0.34 mm and 0.94 mm, for the inner and the outer coil leg, respectively.

1.3.2 2D mechanical analysis

A detailed FE 2D model has been analysed for the inner leg at equatorial plane, in order to check the stress in the WP at the conductor detail level, i.e. beyond the smeared properties assumption used within the 3D global model described in the previous paragraph. The WP is analysed in plane strain approximation, with a mesh of 46953 triangular parabolic elements and 95120 nodes. Boundary conditions are: cyclic symmetry at wedging, where displacements normal to the surface are suppressed, and frictionless contact between node pairs at WP and casing whose displacements normal to the contact surface are linked. The detachment of the WP from the casing on the plasma-facing side is allowed, as can be inferred from Figure VII (upper left panel), where the 2D analysis output is shown, in terms of deformation and global Von Mises stresses. Peak stress values of 830 MPa, are present, but in very small and localized zones corresponding to the jacket inner corner radius (Figure VII, upper right). This is not considered a critical issue at this stage of the design, as there is margin to reshape the conductor corner in the safe direction.

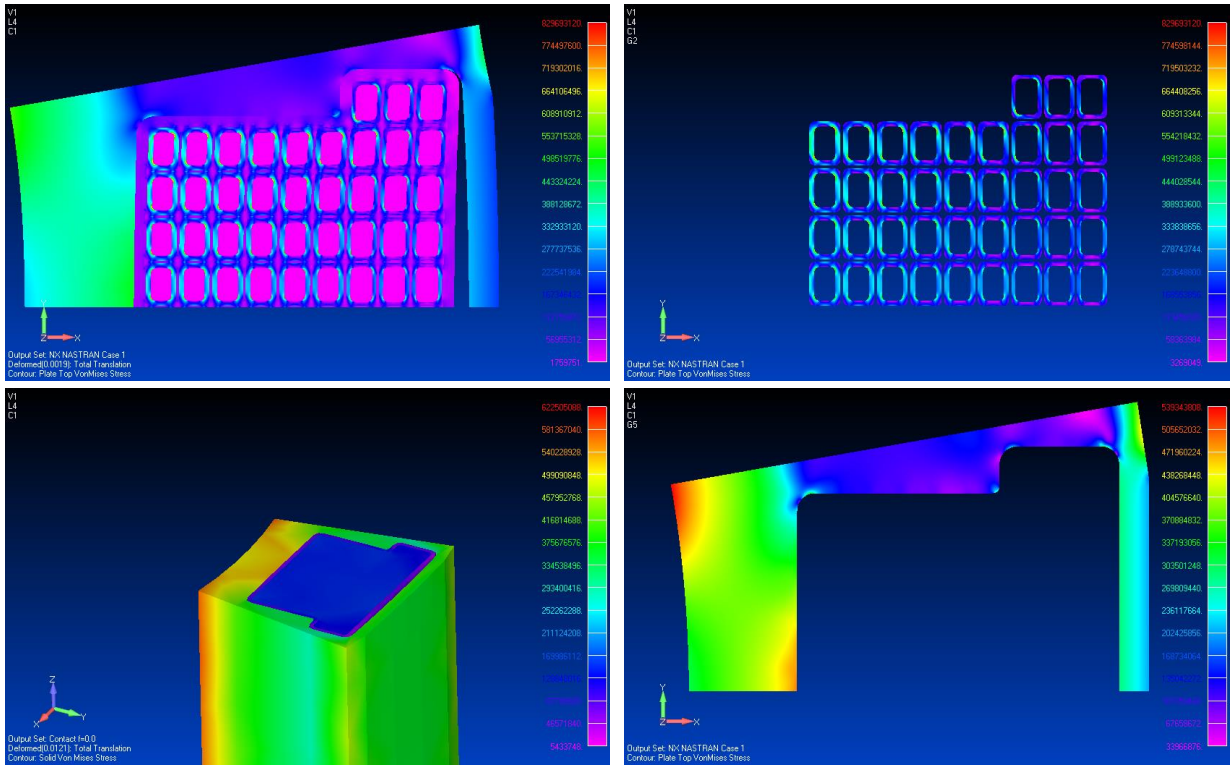


Figure VII. Upper: (2D model) Von Mises stresses global view (left) and stresses on conductor jacket (right). Lower: Von Mises stresses in the TF inner leg at equatorial plane, from 3D (left) and 2D (right) analysis.

As outcome of the mechanical analyses carried out so far, no major issue is foreseen for the present TF coil design proposal. Further and more complete analyses, including out-of-plane forces and cool-down effects, will be carried out in the near future.

1.4 TF - Inductance calculation

To estimate the inductance values of the TF coil system, a 3D magneto-static simulation study in COMSOL Multiphysics® environment has been carried out. The software, using AC/DC module, solves the magnetic fields surrounding the coils and calculates the inductances. Geometry of this study is created in 3D space dimension and consists of 20 domains: one plasma domain, one air domain surrounding the TF coils and the remaining ones are coil domains. The effects of central solenoid and poloidal field coils are not considered in this first study. As material of TF conductors and plasma region, they have been approximated as made of copper, having a conductivity $\sigma = 5.998 \text{ E}+07 \text{ S}\cdot\text{m}^{-1}$ (thus with characteristic properties at 4.2 K), and air, respectively. Each TF coil has been modelled considering the winding pack only, as the DC current carrying element, with $I_{\text{coil}} = 3.6 \text{ MA}$. The plasma current has not been considered in the present study ($I_{\text{plasma}} = 0$).

Total magnetic energy for the 18 coils is $W_m = 1.96$ GJ, and the total inductance value is calculated from the total magnetic energy using the classic formula $W_m = (1/2) * L * I^2$. The same applies for one single TF coil. In this way, the calculated self-inductance values for the single TF coil and the whole TF coil system are:

$$L_{\text{coil}} = 41 \text{ mH}$$

$$L_{18 \text{ coils}} = 1.83 \text{ H}$$

1.5 TF - ripple

The Toroidal Field (TF) ripple is defined as $\frac{\max(B_\phi(\phi)) - \min(B_\phi(\phi))}{\max(B_\phi(\phi)) + \min(B_\phi(\phi))}$, where ϕ indicates the toroidal angle; it is

computed resorting to the CARIDDI code [34][34]. For the computation, different assumptions have been made. Two slightly different shapes of the coil (“nominal” and “modified”, respectively) were considered during a preliminary optimization phase. The difference between the two shapes is shown in Figure VIII(a), in terms of the outermost winding pack contour. The “nominal” shape refers to the coil layout analysed throughout the rest of the paper. The radial extension of the winding pack is maintained at its value of 0.35 m but concerning its toroidal extension, either the nominal configuration is used, as shown in Figure II (named “wedge” winding pack configuration in the following), or a simplified rectangular winding pack has been considered (“rectangular” configuration in the following). The overall mesh of the current carrying elements is reported in Figure VIII(b), together with the separatrix of the plasma. A total of 18 TF coils have been distributed around the torus.

The results for various cases are reported in Table 1-IV. Figure IX refers to non-optimal case (c) of Table 1-IV. The maximum ripple is found in the outboard region and it varies from around 0.6% to around 1.22%, depending on the considered model. For the present design, i.e. nominal coil in “wedge” condition, a maximum ripple of 0.99% is calculated.

TABLE 1-IV
TF RIPPLE FOR VARIOUS CASES

Case	Winding pack	TF coil trace	Maximum ripple
(a)	Rectangular	Nominal	1.22%
(b)	Rectangular	Modified	0.74%
(c)	Wedge	Nominal	0.99%
(d)	Wedge	Modified	0.62%

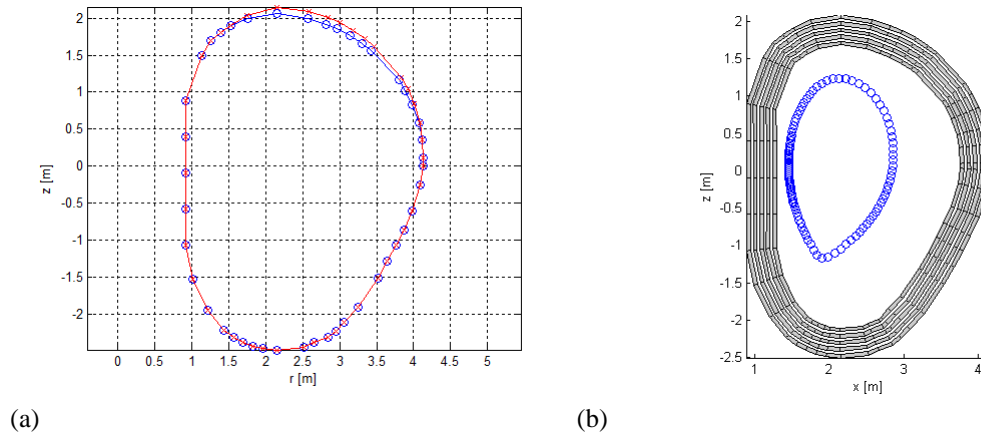


Figure VIII: TF coil contour at the outermost winding pack edge (a) with the nominal, blue empty points, and modified, red crosses, traces; the 3D mesh view with the nominal separatrix (b).

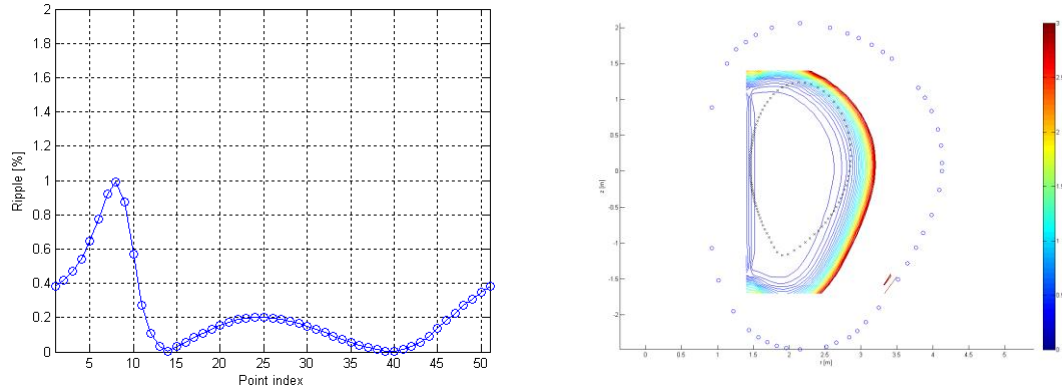


Figure IX: TF ripple at the plasma separatrix; the points are numbered counterclockwise, starting from outboard mid-plane.

2 DTT Poloidal Field coil system

The design of the whole poloidal field coil system is based on the most conservative assumption of imposing to the conductor the highest magnetic field and the highest current ever reached in any of the analysed scenarios, even when these two conditions would not occur simultaneously.

The CS assembly consists of a stack of six solenoids (CS3U to CS3L), 4 of which (CS2U to CS2L) are characterized by an height of 0.97 m, the outermost ones CS3U and CS3L being 0.64 m in height. Radial extension is the same for all, with inner diameter 1.34 m and thickness 0.34 m. Such dimensions are the best compromise for maximizing the available magnetic flux while reducing the required superconductor cross-section. A pre-compression structure is also foreseen for the whole CS pack.

The external poloidal field (PF) system is made of 6 independent circular coils, with inner diameters ranging from 2.68 m (for PF1) to 8.56 m (for PF3). They are clamped to the TF coils, where also their weight is supported.

The eight In-vessel coils (C1 to C8) are made of a single layer of insulated copper conductor, in a size ranging from 70 x 70 mm to 140 x 140 mm. The coils diameters range from 2.88 m (C1) to 6.98 m (C6).

2.1 CS coil description

The DTT Central Solenoid operates at a peak field of 12.5 T, so it relies on Nb_3Sn as superconducting material. Qualitatively the CS conductor is similar to that of the TF coil: a rectangular Cable-in-Conduit conductor, with low void fraction, long twist pitch cable configuration, and no cooling channel for the circulation of supercritical helium. Considering the intrinsic ramping operation of the CS coil, some specific features of the CICC will need to be investigated, in order to maintain the AC losses to a manageable level (see Section 2.2 below). With respect to the CICC for the TF coil, this will be achieved by adding steel wrappings around the last-but-one cabling stages and/or by relaxing the strict condition on the maximum allowed void fraction in its section. Such solutions will however need to be verified, possibly through a design qualification sample test, in order to better assess the trade-off between the requirements on heat loads due to AC losses, and those of the DC performance.

The magnet is made of 6 stacked and independent modules. Its assembly is shown in Figure X, and relies on upper and lower centring systems, connected to the TF coil and providing support against horizontal forces.

The CS weight and any net vertical force component are transmitted to the TF coil structures, through gravity supports. The magnetic hoop forces during operation are reacted internally, within the winding, by the conductor jacket. A system of flanges and tie plates provides the axial pre-compression to the stack of modules.

The six modules can be energized independently, according to plasma formation and shaping requirements.

The modules will be pancake-wound and each single pancake will be made of 15 conductor turns, corresponding to a conductor unit length of about 63 m. Each of the 4 central modules will be constituted of 420 turns, whereas the uppermost and lowermost modules (CS3U and CS3L, respectively) are made of 270 turns each. Total number of turns in CS coil is thus 2220, and total current is 51 MAtturns. Due to this relatively short length, conductors can be wound in hexa-pancakes, still avoiding the use of a pressure relief channel inside the CICC. The hydraulic length of a hexa-pancake would in fact be quite short (about 190 m), so that the pumping load on the cryogenic plant can be kept within small levels, with an operating mass flow rate of 1.5 g/s per cooling path. In particular, each of the CS3U and CS3L modules will be made of 3 hexa-pancakes, whereas each of the CS1U,

CS1L, CS2U, and CS2L modules will be made of 4 hexa-pancakes, and two double-pancakes at the upper and lower extremities. The CS coil will thus be made of 60 parallel hydraulic paths, with the 30 inlet pipes located inside the coil bore, and for a total of 90 g/s of supercritical helium, circulating at about 6 bar inlet pressure. A separation layer of 32 mm is left between modules, to accommodate an insulation layer and hydraulic pipes. The overall CS system will include 24 inter-pancake joints and 12 terminations. Inter-pancake joints of the “ENEA-type” [6] shall be manufactured in-line during winding and will be completely embedded within the coil structures, whereas the terminal joints will be placed in the outer coil region. As anticipated for TF, this joint layout has been previously adopted in other projects [6], [8], and it is currently used also in the ITER CS coil [9]. Bus-bars and helium pipes run outside the coil, within the room available between the external CS coil surface and the TF coil surface. An artistic view of the CS coil assembly is shown in Figure X: the 6 modules are identified with different colours, for clarity.

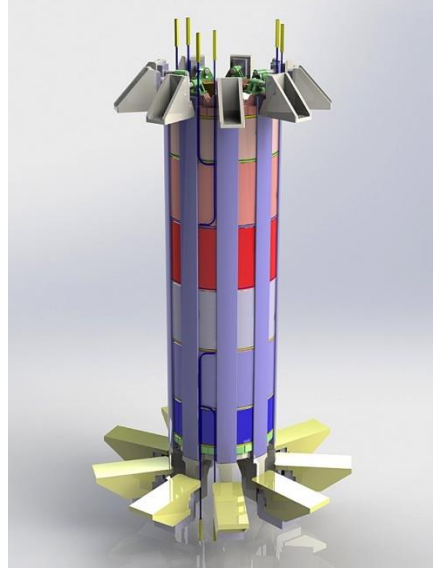


Figure X: DTT CS coil assembly (artistic view).

The main conductor features and operating conditions are summarized in Table 2-I.

TABLE 2-I
CS CONDUCTOR MAIN PARAMETERS

Operating current	23.0 kA
Peak magnetic field	12.5 T
Minimum Temperature Margin	1.5 K
Cumulative operating load	288 kN/m
# Nb3Sn strands	360
# Cu segregated strands	90
Cu and Nb3Sn Strand diameter	0.82 mm
Strand Cu:nonCu ratio	1
Non-Cu current density	242 A/mm ²
He Inlet Temperature	4.5 K
Conductor outer dimensions	31.6 mm x 19.8 mm
Jacket Thickness (316LN)	2.9 mm
Cable area	353 mm ²
Void Fraction	26%
Steel section per turn (jacket)	242.4 mm ²

A simplified computation of the hotspot temperature reached during a quench has been carried out, within an adiabatic 0D model [17]. Figure XI shows the result, in terms of temperature evolution with time, after a quench occurring at t=0. Here the two reference cases considered are: a) heat absorbed totally by copper and

superconducting wires only (red curve in figure), for which the ITER design criterion would be: $T_{\text{hotspot}} < 250$ K; b) heat absorbed by all materials components within the conductor, including the jacket steel and helium (blue curve in figure), where $T_{\text{hotspot}} < 150$ K should hold. For this calculation, a quench detection delay time constant: $\tau_{\text{delay}} = 2$ s has been considered, and a coil discharge time constant: $\tau_{\text{discharge}} = 10$ s.

As the result shows, the hotspot values are well within the ITER reference design criteria, so that the Cu cross-section inside the cable might also be reduced in a possible future design refinement.

Further checks are on the other hand required, to verify the CS winding pack mechanical behaviour during electro-magnetic loading, since this may present some critical aspects.

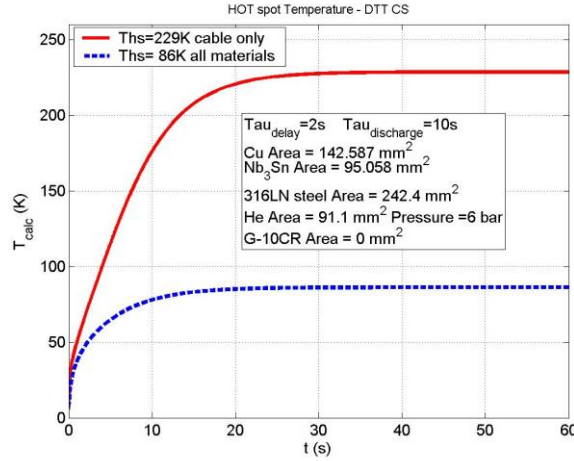


Figure XI: Hotspot calculation for DTT CS conductor during a quench.

2.2 CS - AC losses

In any CS system, intrinsically operating in a variable current mode, a critical aspect is the possibility to sustain the heat load due to AC losses, still maintaining a sufficient temperature margin.

The assessment of the power losses generated in variable regime, generically referred to as AC losses, is necessary to define the requirements on the strand filament diameter, d_{eff} , and on specific conductor design features, as *e.g.* the presence of sub-cable wrapping of the void fraction value.

The three contributions to AC losses have been calculated: the hysteresis losses, Q_{hyst} , derived from the irreversible magnetization due to the pinning of fluxoids arising when the external magnetic field B is swept; the coupling losses, Q_{coup} , ascribed to the coupling currents in multi-filamentary wires and multistage cables, which flow in the superconducting material and close through the normal metal (where Ohmic dissipation takes place); and the eddy current losses, Q_{eddy} , which we consider to take place only in the cable jacket. For the sake of simplicity, in this model we will assume a single effective time constant for coupling losses, thus neglecting the actual multistage cable layout. On the contrary, Q_{hyst} is assumed to be independent on the rate of change of the applied field.

We assume that the system can be described in terms of isolated cylindrical wires in transversal field and, in order to simplify the computations, we consider a quasi-static regime (*i.e.*, slow varying fields with respect to the time scale of transients) in which the internal and external field variations are related through the expression $B_e = B_i + n\tau dB_i/dt$, [17], [35], where B_e and B_i are the external applied field and the induction field inside the cable, respectively, whereas $i = \frac{I_t}{I_c}$, n is a geometrical factor ($n = 2$). We further assume that $B_i \approx B_e$ and hence $\dot{B}_e = \dot{B}_i$.

For the present study we consider the DDT reference scenario for the CS coils, which can be divided in 4 main phases: charge of the coil (in 300 s), fast ramp down of the field (in 27 s), flat top (100 s long) and final discharge of the coil (in 300 s). We take $n\tau = 55$ ms and $d_{\text{eff}} = 5$ μm as values representative for the time constant and the filament size, respectively [18]. The overall loss results for the CS conductor are summarized in **Errore. 'origine riferimento non è stata trovata..** Coupling losses are more than four times larger than hysteresis losses, as expected, whereas the eddy currents on the jacket can be neglected.

TABLE 2-II
TOTAL AC LOSSES BY CS REFERENCE SCENARIO

Q_{hyst} (kJ)	Q_{coup} (kJ)	Q_{eddy} (J)	Q_{TOT} (J)
19.1	68.5	9	87.6

These numbers appear to be within manageable levels and the designed conductor seems to be adequate to sustain the expected AC losses, even if a detailed thermo-hydraulic assessment of the conductor cooling capability and AC losses requirements needs to be carried out.

The total power loss evolution in time is reported in Figure XII along with breakdown into the hysteresis, coupling and eddy current contributions.

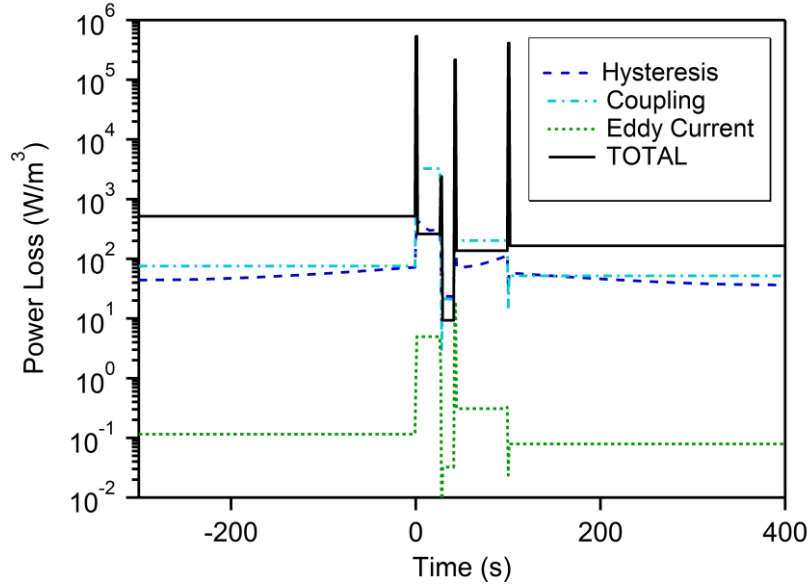


Figure XII: Total power loss and contributions due to various mechanisms, vs. time in the highest field pancake.

2.3 CS - mechanical analysis

A 2D finite element model of the CS magnet has been developed in ANSYS®, to simulate the magneto-structural response of the CS under operating conditions, taking advantage of the axial symmetry of the structure. In this preliminary analysis, the only applied load is represented by the Lorentz forces caused by feeding all the modules at the maximum current simultaneously. The magnetic field map has been calculated by ANSYS® and then applied, in terms of Lorentz forces, as a body load onto the structural mesh. For the sake of simplicity, all materials are considered to be in elastic linear field and isotropic. In the developed FE model, the CS modules are considered to be perfectly bonded.



Figure XIII: Insulation layer induced maximum shear stress.

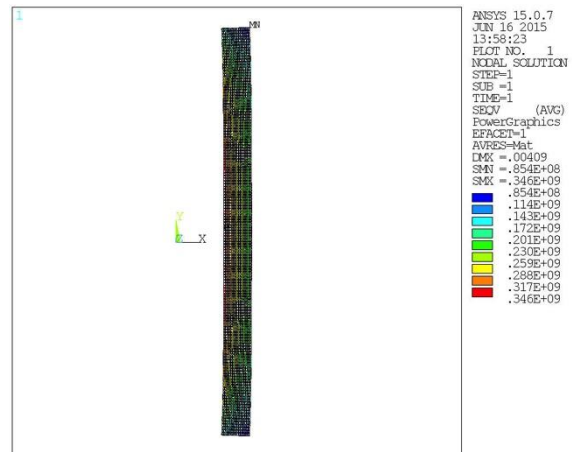


Figure XIV: SS jacket induced von Mises stress.

The FE analyses, reported in Figure XIII and in Figure XIV, show that the stress conditions are below critical values: using the Von Mises yield criterion, the maximum stress induced in the 316LN SS jacket is about 346 MPa ($\sigma_{VM,jacket}$), as shown in Figure XIV, thus well below the yield stress for 316LN, which is about 900 MPa

at 4.2 K; the induced shear stresses into the insulation layer ($\tau_{\text{insulation}}$) reaches a maximum value of 9 MPa (as shown in Figure XIII), well below the maximum allowable for this specific material: $\tau_{\text{max.insul.}}=50$ MPa.

From the structural point of view, under the assumptions introduced to implement the model, the FE analysis performed in the mentioned conditions give positive results, showing that no major issue is present. These results shall be confirmed by more detailed analyses, which are still on-going.

2.4 PF - description

The 6 Poloidal Field (PF) coils are all constituted of NbTi CICC, and operate at lower field with respect to those of ITER. Maximum field is on the PF6, and is 4.0 T; the lowest one is on the PF3, and is of 2.3 T. The differences in the design of the 6 CICC constituting the 6 coils are mainly driven by the need to find the best trade-off between the room availability and the requested performances. The reference NbTi performances are those of JT-60SA strands [36], characterized by a diameter of 0.81 mm and Cu:nonCu = 1.9. All conductors are slightly rectangular, as for the TF and CS CICC, and will be manufactured through deformation by lamination of a round tube, inside which the cable will be inserted.

In Table 2-III, a summary of the 6 Cable-in-Conduit conductor characteristics is reported.

TABLE 2-III
PF COILS CONDUCTORS

	PF1	PF2	PF3	PF4	PF5	PF6
B_{peak} (T)	3.7	3.0	2.4	3.4	3.9	4.0
I_{op} (kA)	25.2	22.6	21.2	24.7	23.0	23.3
Computed ΔT_{margin} (Tinlet = 4.5K)	1.6	1.9	2.3	1.9	1.5	1.6
Ext. dimensions (mm)	29 x 32	26 x 29	24 x 35	24.5 x 33.5	26 x 28.5	29 x 32
Jacket thickness (mm)	4	3.5	3.5	3.5	3.5	4.0
Turn insulation thickness (mm)	1.0	1.0	1.0	1.0	1.0	1.0
NbTi strand #	90	72	72	90	72	90
Cu strand #	396	306	360	342	306	396
Void Fraction (%)	32.2	35.5	36.2	34.5	33.8	32.2
Total Conductor Length (km)	1.1	2.4	3.1	3.7	3.2	2.5
Hydraulic Length (km)	0.15	0.40	0.22	0.26	0.39	0.25

The conductors for winding the PF1 and the PF6 coils are identical. A further optimization study is required in order to decrease the differences among the other conductors, for the sake of costs saving.

Due to the relatively high hydraulic lengths, despite the high void fraction values foreseen, the introduction of a central channel for pressure relief, presently not foreseen, is currently under study, in particular for the PF2-5 conductors. Further analyses, in particular to define the maximum limits for the quench behaviour and the AC losses load, are on-going to optimize the present design.

The coils will be wound in Double-Pancakes, with the He inlet placed close to the area where the magnetic peak field is located, which is about at the half of the single unit length. An additional > 3 mm thick glass-reinforced epoxy-resin layer for ground insulation is foreseen around the windings.

The PF coils are placed into clamps fixed to the TF coil structure through shelves, which will allow the radial movements linked to their energization.

2.5 CS & PF - magnetic field analysis

The magnetic field analysis has been performed by TOSCA[®] code for the complete PF and CS coils system. It has been calculated for each poloidal coil at all instants of the Reference Scenario (RS) as well as for Start-of-Flat-Top (SOF) and End-of-Flat-Top (EOF) of alternative scenarios, like the so-called “snowflake plus” (SF+) and Double Null (DN) configurations [37], to evaluate the maximum field for a safe design of the conductors and the winding packs. In the model, the total operating current (MATurns) for each poloidal field coil is flowing in its WP area, while plasma contribution has been included by letting the full plasma current flow in a ring positioned at the plasma major radius.

The maximum operating magnetic field on CS (12.5T) is found at the initial instant of the reference scenario (RS@t=0s), when the CS modules carry the maximum current.

At RS@t=0s, the PF6 coil presents its maximum magnetic field, say 4T, at a current value of 4.301 MATurns, as at SOF of the Double Null alternative configuration, when it operates at its maximum current (6.046 MATurns). This is due to contributions of also the other coils.

Table 2-IV summarizes the results.

TABLE 2-IV
ABSOLUTE MAX CURRENTS AND MAGNETIC FIELDS FOR PF AND CS

	PF1	PF2	PF3	PF4	PF5	PF6	CS3U	CS2U	CS1U	CS1L	CS2L	CS3L
B_{\max} (T)	3.7	3.0	2.4	3.4	3.9	4.0	11.8	12.5	12.5	12.5	12.5	9.8
I_{\max} (MATurns)	3.277	2.446	2.371	3.454	3.337	6.046	6.028	9.748	9.748	9.748	9.748	5.726

2.6 In-Vessel copper Coils

The poloidal field system of DTT also includes eight in-vessel coils made with a single layer of insulated copper conductor (Figure XV), in a size ranging from 70 x 70 mm to 140 x 140 mm (Table 2-V):

- 2 in-vessel coils for radial and vertical stabilization and control
- 4 out of 6 in-vessel coil (IVC) for magnetic control of Scrape Off Layer and strike point sweeping

In-vessel coils C5-C6 can effectively be used for plasma radial control and vertical stabilization [38][39], [38]. They are also used in the breakdown phase to produce a 6 mT vertical field. In-vessel coils C1-C4 are capable to locally modify the magnetic field in the vicinity of the divertor target [37]-[39], and are therefore fundamental in view of the study of the divertor physics and technology which is one of the main target of the DTT project. These internal coils will be used for optimizing the local magnetic configuration and consequently controlling various parameters related to the power exhaust (flux expansion, connection length, distance between null points, etc.). In-vessel coils C1-C4, as well as C7-C8, can also be used for plasma wobbling or strike point sweeping (in any case no more than 4 internal coils will be fed in addition to C5-C6 during a pulse). The calculations show that 120 kA in C1 and C3 connected in anti-series would yield 64 mm sweeping on the outer strike point and 42 mm on the inner one. However, there are some side effects outside the vacuum vessel (e.g., 25 kATurns induced in PF6).

Optimization of frequency and currents for strike point sweeping is planned in the future.

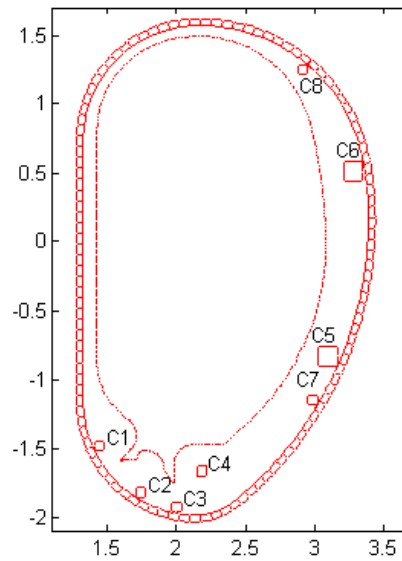


Figure XV: In-vessel copper coils.

TABLE 2-V
IN-VESSEL COPPER COILS: GEOMETRY AND VOLTAGE/CURRENT LIMITS (FOUR QUADRANTS)

Name	R (m)	Z (m)	ΔR (m)	ΔZ (m)	Turns	I_{sat} (kA)	V_{sat} (V)
C1	1.44	-1.481	0.07	0.07	1	60	50
C2	1.74	-1.823	0.07	0.07	1	60	50
C3	2	-1.925	0.07	0.07	1	60	50
C4	2.18	-1.668	0.07	0.07	1	60	50
C5	3.1	-0.83	0.14	0.14	4	25	200
C6	3.285	0.51	0.14	0.14	4	25	200
C7	2.988	-1.15	0.07	0.07	1	60	50
C8	2.915	1.25	0.07	0.07	1	60	50

The forces on the in-vessel coils are scaled from ITER [40], where the maximum force is 744 kN/m and the maximum current is 240 kA (up to 320 kA in short transients). Since in DTT we assume 60 kA, the maximum force should be reduced to 186 kN/m. Therefore, a limit of ± 4 MN for the vertical force is taken for the coils connected to other structures (vacuum vessel or divertor) via rails or other means.

The thermal analysis shows that a current limit of 60 kA is largely compatible with steady state operations with a proper cooling system. There is also the possibility of doubling the cross section and the current limit with an outlet conductor temperature not exceeding 150°C [37].

Conclusions

The magnet system of the DTT tokamak reactor proposal has been designed and its main characteristics have been investigated proving its feasibility. The 18 superconducting Toroidal Field coils are layer wound using two grades of Nb₃Sn rectangular cable-in-conduit-conductors (CICC), with low void fraction. The high- and low-field CICC's operate at 46.3 kA, but in a peak field of 11.4 T and 7.6 T, respectively. The 6 Central Solenoid modules are wound in pancakes, and are also based on a rectangular Nb₃Sn CICC, but operating at 12.5 T and 23 kA. Also the PF coil system is made of superconducting CICC's, but using NbTi wires. Operating currents and field for the 6 coils are in the range 21 kA ÷ 25 kA and 2.4 T ÷ 4 T, respectively. Finally, a system of 8 resistive in-vessel coils are designed to allow radial and vertical stabilization and control of the plasma, as well as the magnetic control close to the divertor region. Though a more detailed study is mandatory before proceeding to the engineering and a possible construction phase, the present work shows that no major issue or killing factors have been identified. A risk assessment, not reported in the present paper, has been developed as well, covering all the main aspects that could delay the project or reduce the machine performance.

References

- [1] G. Federici et al., "Overview of the design approach and prioritization of R&D activities towards an EU DEMO", Fusion Engineering and Design, vol. 109-111, Part B, pp. 1464-1474, Nov. 2016
- [2] M.L. Apicella, S.Ciattaglia, A. Colangeli, G.Maddaluno, G.Mazzitelli, D.Marocco, R. Villari, "The DTT device: safety, fuelling and auxiliary system", submitted to Fusion Engineering and Design, Special Issue for DTT (2017)
- [3] V. Corato *et al.*, "Common operating values for the DEMO Magnet design for 2016," EUROfusion IDM server, <http://www.euro-fusionscipub.org/archives/eurofusion/common-operating-values-for-demo-magnets-design-for-2016-2>, September 2016.
- [4] L. Muzzi, G. De Marzi, A. Di Zenobio and A. della Corte "Cable-in-conduit conductors: lessons from the recent past for future developments with low and high temperature superconductors", Topical Review, Supercond. Sci. Technol. 28 (2015) 053001 (25pp)
- [5] L. Muzzi et al., "Design, manufacture and test of an 80 kA-class Nb₃Sn cable-in-conduit conductor with rectangular geometry and distributed pressure relief channels", IEEE Trans. Appl. Supercond., submitted for publication.
- [6] A. Di Zenobio et al. , Joint Design for the EDIPO, IEEE Trans. Appl. Supercond. 18 (2008) 192
- [7] A. Portone et al., "Design and Procurement of the European Dipole (EDIPO) Superconducting Magnet", IEEE Trans. Appl. Supercond. , Vol. 18,499 – 503, No. 2, June 2008
- [8] V. Corato et al., "Detailed design of the large-bore 8 T superconducting magnet for the NAFASSY test facility", Supercond. Sci. Technol. 28 (2015) 034005 (9pp)
- [9] N. Martovetsky, A. B. Berryhill, and S. J. Kenney, "Qualification of the Joints for the ITER Central Solenoid", IEEE Trans. Appl. Supercond. , vol. 22, no. 3, Art. ID 4804004, June 2012.
- [10] A. Devred et al. "Challenges and status of ITER conductor production" Supercond. Sci. Technol. **27** (2014) 044001 (39pp)
- [11] D. Bessette et al., "Design of a Nb₃Sn CICC to withstand the 6000 electromagnetic cycles of the ITER Central Solenoid", IEEE Trans. Appl. Supercond., Vol. 23 (2015) 4200505
- [12] A. della Corte et al., "Successful performances of the EU-AltTF sample, a large size Nb₃Sn cable-in-conduit conductor with rectangular geometry", Supercond. Sci. Technol. 23 (2010) 045028 (6pp)
- [13] I. R. Dixon et al., 2009 IEEE Trans. Appl. Supercond. 19 1462; Dixon I. R. et al. , 2012 IEEE Trans. Appl. Supercond. 22 4301004
- [14] S. A. J. Wieggers et Al., "Conceptual Design Of The 45 T Hybrid Magnet At The Nijmegen High Field Magnet Laboratory", IEEE Trans. Appl. Supercond. , Vol. 20, No. 3, 688 – 691, June 2010
- [15] P. Bruzzone et al., "Test Results of a Nb₃Sn Cable-in-Conduit Conductor With Variable Pitch Sequence, IEEE Trans. Appl. Supercond. **19** (2009) 1448
- [16] K. Sedlak et al., "Test of the MF-CICC Conductor Designed for the 12 T Outsert Coil of the HFML 45 T Hybrid Magnet", IEEE Trans. Appl. Supercond. (2016), accepted for publication
- [17] M. N. Wilson, "Superconducting Magnets (Monographs on Cryogenics)", Oxford University Press, New edition (1987)
- [18] P. Bauer, H. Rajainmaki, E. Salpietro, "EFDA Material Data Compilation for Superconductor Simulation", (2007)
- [19] G. Di Gironimo et al., "The DTT device: first wall, vessel and containment structure", submitted to Fusion Engineering and Design, Special Issue for DTT (2017)
- [20] L. Savoldi Richard, F. Casella, B. Fiori and R. Zanino, The 4C Code for the Cryogenic Circuit Conductor and Coil modeling in ITER, Cryogenics 50 (2010) 167-176
- [21] R. Bonifetto, T. Isono, N. Martovetsky, L. Savoldi and R. Zanino, Analysis of the DC performance of the ITER CSI coil using the 4C code, submitted to Fusion Engineering and Design (2016)
- [22] R. Bonifetto, P.K. Domalapally, G.M. Polli, L. Savoldi Richard, S. Turtù, R. Villari and R. Zanino, Computation of JT-60SA TF coil temperature margin using the 4C code, Fusion Engineering and Design 86 (2011) 1493-1496
- [23] L. Savoldi Richard, R. Bonifetto, U. Bottero, A. Foussat, N. Mitchell, K. Seo and R. Zanino, Analysis of the effects of the nuclear heat load on the ITER TF magnets temperature margin, IEEE Transactions on Applied Superconductivity 24 (2014) Art. ID 4200104
- [24] R. Zanino, R. Bonifetto, O. Dicuonzo, L. Muzzi, G. F. Nallo, L. Savoldi and S. Turtù, Development of a Thermal-Hydraulic Model for the European DEMO TF Coil, IEEE Transactions on Applied Superconductivity 26 (2016) Art. ID 4201606

- [25] L. Savoldi, A. Brighenti, R. Bonifetto, V. Corato, L. Muzzi, S. Turtù and R. Zanino, Performance analysis of a graded winding pack design for the EU DEMO TF coil in normal and off-normal conditions, submitted to IEEE Transactions on Applied Superconductivity (2016)
- [26] S. Turtù, private communication, October 2016
- [27] R. Villari, Nuclear heating of FAST TF superconducting magnets, *ENEA Report*, 8 June 2010
- [28] L. Bottura and B. Bordini, Jc (B, T, ϵ) Parameterization for the ITER Nb₃Sn Production, IEEE Transactions on Applied Superconductivity 19 (2009) 1521-1524
- [29] M. Lewandowska and M. Bagnasco, Modified friction factor correlation for CICC's based on a porous media analogy, Cryogenics 51 (2011) 541-545
- [30] P. Decool, et al., JT-60SA TF Coils: Experimental Check of Hydraulic Operating Conditions, IEEE Transactions on Applied Superconductivity 26 (2016) Art. ID 4201705
- [31] L. Zani and U. Fischer, Advanced definition of neutronic heat load density map on DEMO TF coils, EFDA_D_2MFVCA, 18/10/2014, unpublished document.
- [32] ITER Design Description Document DDD11-Magnets, Section 2-TF Coils and Structures, ITER_D_2MVZNX v2.2, Sept. 2009"
- [33] M. E. Biancolini, C. Brutti, F. Giorgetti, L. Muzzi, S. Turtù, A. Anemona "A new meshless approach to map electromagnetic loads for FEM analysis on DEMO TF coil system" Fusion Engineering and Design, Vol. 100, Nov. 2015, Pages 226–238.
- [34] R. Albanese, G. Rubinacci, "Finite element methods for the solution of 3D eddy current problems", Adv. Imaging Electron Phys. 102 (1998) 1–86.
- [35] G. Ries, IEEE Trans. Magn.13, 524 (1977)
- [36] L. Zani, P. Barabaschi, E. Di Pietro, and M. Verrecchia, "Completion of TF Strand Production and Progress of TF Conductor Manufacture for JT-60SA Project", IEEE Trans. Appl. Supercond. , vol. 24, no. 3, Art. ID 6000105, June 2014
- [37] R. Ambrosino et al., "The DTT device: alternative configurations", submitted to Fusion Engineering and Design, Special Issue for DTT (2017)
- [38] Fusion Electricity, EFDA – A roadmap to the realisation of fusion energy, November 2012 (http://users.euro-fusion.org/iterphysicswiki/images/9/9b/EFDA_Fusion_Roadmap_2M8JBG_v1_0.pdf)
- [39] M. Valisa et al., "The DTT device: data acquisition, diagnostics and control". Submitted to Special Issue of Fusion Engineering and Design entitled "DTT: Divertor Tokamak Test facility" to be published in early 2017
- [40] X. Wang, Xianwei, F. Xie, and H. Jin. "Electromagnetic Analysis of the ITER Upper VS Coil". Journal of Superconductivity and Novel Magnetism, Vol. 27, Issue 4 (2014), pp. 1015-1019.